The Mechanism of Target Base Attack in DNA Cytosine Carbon 5 Methylation†

Željko M. Svedružić‡ and Norbert O. Reich*

Department of Chemistry and Biochemistry, University of California, Santa Barbara, California 93106

Received February 12, 2004; Revised Manuscript Received July 1, 2004

ABSTRACT: We measured the tritium exchange reaction on cytosine C^5 in the presence of AdoMet analogues to investigate the catalytic mechanism of the bacterial DNA cytosine methyltransferase M.HhaI. Poly(dG-dC) and poly(dI-dC) substrates were used to investigate the function of the active site loop (residues 80−99), stability of the extrahelical base, base flipping mechanism, and processivity on DNA substrates. On the basis of several experimental approaches, we show that methyl transfer is the rate-limiting pre-steady-state step. Further, we show that the active site loop opening contributes to the rate-limiting step during multiple cycles of catalysis. Target base activation and nucleophilic attack by cysteine 81 are fast and readily reversible. Thus, the reaction intermediates involving the activated target base and the extrahelical base are in equilibrium and accumulate prior to the slow methyl transfer step. The stability of the activated target base depends on the active site loop closure, which is dependent on the hydrogen bond between isoleucine 86 and the guanine 5′ to the target cytosine. These interactions prevent the premature release of the extrahelical base and uncontrolled solvent access; the latter modulates the exchange reaction and, by implication, the mutagenic deamination reaction. The processive catalysis by M.HhaI is also regulated by the interaction between isoleucine 86 and the DNA substrate. Nucleophilic attack by cysteine 81 is partially rate limiting when the target base is not fully stabilized in the extrahelical position, as observed during the reaction with the $Gln^{237}Trp$ mutant or in the cytosine C^5 exchange reaction in the absence of the cofactor.

Enzymatic pyrimidine methylation is essential for diverse biological pathways including gene regulation, DNA and RNA biosynthesis, DNA repair, and protection against foreign DNA (*1*−*3*). Not surprisingly, the folate- and *S*-adenosylmethionine-dependent methyltransferases involved in these processes are the targets of antibiotics, cancer chemotherapies, and other drugs (*4*, *5*). Enzymatic activation of the pyrimidine ring occurs by various mechanisms, with the single common feature being formation of a covalent intermediate between the enzyme and the pyrimidine C^6 position. *S*-Adenosylmethionine-dependent DNA cytosine methyltransferases represent a broad, structurally and mechanistically characterized family of enzymes (*4*). M.HhaI[1] (methyltransferase *Haemophilus haemolyticus* type I) was the first AdoMet-dependent enzyme to be structurally characterized (*6*, *7*) and provides a paradigm not only for AdoMet-dependent enzymes but for enzymes that induce dramatic conformational changes within their duplex DNA substrate (*8*, *9*). M.HhaI methylates the underlined cytosine in duplex DNA (G<u>C</u>GC), stabilizing the cytosine into an extrahelical position residing within the active site of the enzyme (Figure 1).

FIGURE 1: Four steps leading to methylation or exchange by DNA cytosine methyltransferases. The exchange reaction is proposed to share all steps up to the transfer of a proton in place of a methyl moiety. The equilibrium steps up to and including covalent adduct formation are implied by the results in this work.

Formation of the ternary M.HhaI·DNA·AdoMet complex is followed by at least three steps leading to product formation, outlined in Figure 1: base flipping, covalent adduct formation, and methyl transfer. We and others have studied this process in detail for M.HhaI (*9*, *10*), as well as other DNA methyltransferases (*11*, *12*). In contrast to the detailed structural information available for M.HhaI (*8*), little is known about the kinetics of these steps. For example, the flipping and methyl transfer kinetics have been directly measured for M.EcoRI (*11*−*13*), an adenine methyltransferase, but other than similar experiments with mismatched DNA (*14*), no such measurements have been made for M.HhaI. ^{19}F NMR and gel shifting evidence support the existence of two M.HhaI·DNA intermediates involving an extrahelical cytosine, one of which is stabilized by the presence of the cofactor (*15*); however, these experiments provide limited mechanistic insights since they represent largely static descriptions and use 5-fluorocytosine, which

† This work was supported by NIH Grant GM 463333 and NSF Grant MCB-9983125 to N.O.R.

* To whom correspondence should be addressed: e-mail, reich@chem.ucsb.edu; tel, 805-893-8368; fax, 805-893-4120.

‡ Current address: School of Molecular Biosciences, Department of Biophysics and Biochemistry, Washington State University, Pullman, WA 99164.

[1] Abbreviations: AdoMet, *S*-adenosyl-L-methionine; AdoHcy, *S*-adenosyl-L-homocysteine; bp, base pair; C^5, C^2, C^4, etc., carbon 5, carbon 2, carbon 4, etc. of the target base ring; ^{5m}C, 5-methyl-2′-deoxycytosine; dCTP, deoxycytosine triphosphate; poly(dG-dC) or dGdC, double-stranded alternating polymer of deoxyguanine and deoxycytosine; dITP, deoxyinosine triphosphate; M.HhaI, methyltransferase *Haemophilus haemolyticus* type I; M.SssI, methyltransferase *Spiroplasma* sp. type I; poly(dI-dC) or dIdC, double-stranded alternating polymer of deoxyinosine and deoxycytosine; pss, pre steady state: ss, steady state; sin, sinefungin; WT, wild type; N-AdoMet, *N*-methyl-AdoMet.

10.1021/bi0496743 CCC: $27.50
Published on Web 08/19/2004

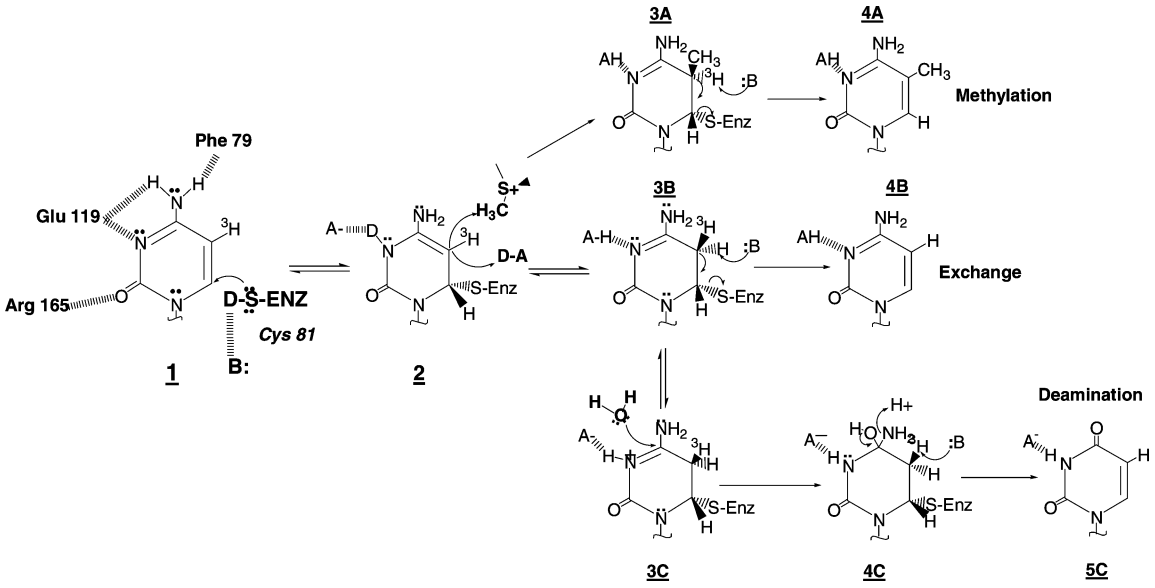

FIGURE 2: Reactions catalyzed by cytosine methyltransferases: methylation (A), ^{3}H exchange (B), and deamination (C). The extrahelical cytosine interacts with active site amino acids that facilitate cysteine 81 nucleophilic attack at cytosine C^6 (intermediate **1**). Nucleophilic attack disrupts the pyrimidine's aromaticity, forming intermediate **2**. Intermediate **2** can readily undergo electrophilic addition, either through methylation (**3A**) or protonation (**3B**). The 5,6-dihydropyrimidine adduct (**3B**) can lead to the exchange reaction (**4B**) or be attacked by water to form intermediate **4C**, which can lead to elimination of NH_3 and mutagenic deamination (**5C**). Acidic groups are labeled as HA and basic groups as :B. All exchangeable protons that can cause SKIE are shown as D in the intermediates (**1** and **2**). ^{3}H exchange rates are measured by acid quench; thus the ^{3}H exchange reaction is detected as soon as intermediate **3A** or **3B** is formed. The methylation reaction is detected as soon as intermediate **3A** is formed. For both reactions the pre steady states are steps that lead to intermediate **3A** (and **3B** for exchange), while the steady-state rates include the subsequent steps (see Methods).

severely perturbs the kinetics of attack and methyl transfer (*10*). Single-turnover measurements with M.HhaI show that the methyl transfer step, or some prior transition, has a rate constant of 0.14−0.26 s^{-1} (*9*, *10*), and the methylation reaction shows a pre-steady-state burst, suggesting that methyl transfer is followed by slow product release steps (*9*, *10*).

We refer to the base flipping and covalent adduct formation as the "target base attack" steps which serve to activate the cytosine to displace the electrophilic methylsulfonium on AdoMet (Figure 2). The proposed mechanism in Figure 2 is based largely on three lines of evidence: (1) structural and mechanistic parallels with the well-studied folate-dependent thymidylate synthetase (*16*), (2) structure−function studies of M.HhaI (*7*, *17*) and other DNA cytosine methyltransferases (*8*), and (3) theoretical studies (*18*). However, details involving individual steps, the identity of the functionalities involved, and the relative contribution to rate-limiting steps remain uncertain. For example, Arg^{165}, Glu^{119}, and Phe^{79} are clearly positioned to interact with the cytosine as shown in Figure 1. Yet, the proposal that the nucleophilic attack by cysteine 81 is assisted by protonation at the cytosine N^3, rather than the cytosine O^2 (*18*) (or both), has no experimental support. Similarly, there is little evidence for the existence, identity, or importance of moieties involved in acid- and base-assisted catalysis to facilitate the β-elimination step (Figure 2). Protein engineering efforts to determine the mechanisms of base flipping and stabilization include the interaction between glutamine 237 and the orphan guanosine (*19*); although the mutants retained function, albeit reduced ~50-fold, the underlying mechanisms were not determined.

M.HhaI catalyzes the exchange of the cytosine C^5 hydrogen (*17*), which is compelling evidence for the proposed mechanism and cysteinylcytosine covalent intermediate (Figure 2). Moreover, because this reaction occurs in the absence of cofactors and is inhibited by *S*-adenosylhomocysteine (*17*), it supports methods of study not suitable for the methylation reaction itself. No evidence for the exchange reaction during AdoMet-dependent steady-state methylation was described for M.HhaI (*17*) or for M.EcoRII, the only other DCMTase studied by this method (*20*); rather, M.HhaI simply replaces the C^5 proton with a methyl group (Figure 2). Bacterial DCMTases catalyze the deamination of cytosine to uracil and of 5-methylcytosine to thymine (Figure 2 and refs *21*−*23*). This mutagenic reaction, if catalyzed by human DCMTases, is postulated to account in part for the high level of CG to TG mutations that occur within critical genes in human cancers (*24*).

We describe pre-steady-state, steady-state, pH, and solvent kinetic isotope effect (SKIE) studies of the methylation and ^{3}H exchange reactions using structural analogues of the DNA and cofactor, AdoMet. The exchange reaction provides unique opportunities because the mechanistic importance of the cofactor can be readily probed with analogues. We used poly(dI-dC) and poly(dG-dC) in our analysis because (i) these substrates allow a quantitative analysis since every enzyme molecule can bind a recognition site and proceed with catalysis, and (ii) the preparation of DNA substrates containing a single radiolabeled [5-^{3}H]cytosine is problematic and provides a less sensitive measure of catalysis (*20*). Poly(dI-dC) and the Gln^{237}Trp mutant provide unique opportunities to study the base flipping step and stabilization of the extrahelical cytosine. Pre-steady-state kinetic, pH, and SKIE studies were used to determine the importance of cysteine 81 toward the rate-limiting events during target base attack, methylation, and exchange.

EXPERIMENTAL PROCEDURES

Materials

S-Adenosyl-L-[*methyl*-^{14}C]methionine (59 mCi/mmol or 131 cpm/pmol), *S*-adenosyl-L-[*methyl*-^{3}H]methionine (66−82 Ci/mmol or 6100−7200 cpm/pmol), deoxy[5-^{3}H]cytidine 5′-triphosphate (19.0 Ci/mmol) ammonium salt, and Sequenase 2.0 were purchased from Amersham Corp. Poly(dI-dC), 1960 bp, dITP, and dCTP were purchased from Pharmacia Biotech. DTT, Trizma, and acid-washed activated charcoal were purchased from Sigma Chemical Co. BSA was purchased from Boehringer Mannheim, and it was DNA free on the basis of the absorbance ratio at 280 and 260 nm. DE81 filters were purchased from Whatman, Inc. Sinefungin was purchased from Sigma Chemical Co. AdoMet (85% pure) was purchased form Sigma Chemical Co. and HPLC purified as described earlier (*25*). WT M.HhaI and the Gln^{237}Trp^{237} mutant were expressed using *Escherichia coli* strain ER1727 containing plasmids pHSHW-5 and pHSH0-1, respectively (generously provided by Dr. S. Kumar, New England Biolabs), and purified as previously described (*9*). The M.HhaI concentration at the end of the preparation was determined by pre-steady-state burst. AdoMet, sinefungin, poly(dI-dC), and poly(dG-dC) concentrations were determined by absorbance at 260 nm. The respective molar absorptivity coefficients are 15.0×10^3 M^{-1} cm^{-1} for AdoMet and its analogues, 6.9×10^3 M^{-1} cm^{-1} for poly(dI-dC) (per bp), and 8.4 10^3 M^{-1} cm^{-1} for poly(dG-dC) (per bp) (Pharmacia Technical Infomation Sheet).

Methods

Preparation of [5-^{3}H]Cytosine−Poly(dI-dC). Labeling reactions were prepared by incubating 500 μM bp poly(dI-dC) with 100 μM [5-^{3}H]dCTP, 1 mM CTP, 10 mM dITP with 0.62 unit/μL Sequenase 2.0 in 40 mM Tris-HCl (pH 7.5), 10 mM $MgCl_2$, 50 mM NaCl, 10 mM DTT, and 1.0 mg/mL BSA. Labeling reactions for [5-^{3}H]cytosine−poly(dG-dC) used the same approach except that poly(dI-dC) was replaced with poly(dG-dC) and 10 mM dITP was replaced by 1 mM dGTP. Reactions were run for 5 h at room temperature. Incorporation of [5-^{3}H]cytosine was followed by spotting the reaction aliquots onto DE81 paper. Spotted papers were washed twice for 5 min in 500 mM KP_i buffer (pH = 6.8) and dried under a heat lamp. The extent of label incorporation was calculated by comparing the counts from unwashed and washed papers. This procedure gives approximately 60% label incorporation. The reaction was stopped by incubating the sample for 5 min at 90 °C followed by slow cooling (2−3 h^{-1}) to room temperature. The cooled sample was centrifuged and the supernatant dialyzed against 10 mM Tris-HCl (pH 8.0) and 10 mM EDTA. The removal of reaction components was determined by comparing the radioactivity from unwashed and washed DE81 papers. The [5-^{3}H]cytosine-labeled poly(dI-dC) and poly(dG-dC) prepared in the described procedure was between 13 and 40 cpm/pmol of base pairs for dIdC,and between 60 and 105 cpm/pmol of base pairs for dGdC.

Methylation Reactions. The methylation reactions were prepared by incubating M.HhaI, DNA substrate, and radioactive AdoMet in 100 mM Tris-HCl (pH 8.0), 10 mM EDTA, 10 mM DTT, and 0.5 mg/mL BSA at 37 °C. The enzyme and DNA concentrations are specific for each assay and are described in the figure legends. Incorporation of [^{3}H]-methyl groups in the DNA substrate was determined as previously described (*25*, *26*). Briefly, the reaction is followed by spotting reaction aliquots on DE81 paper, leading to the detection of intermediate **3A** and all products resulting from its formation (Figure 2). Thus, the pre-steady-state rates are determined by the steps that lead to intermediate **3A** (Figures 1 and 2), while the steady-state rates are determined by steps that follow formation of intermediate **3A**.

Tritium Exchange Reactions. The tritium exchange reaction was followed essentially as previously described (*17*). Briefly, tritium exchange is measured by quenching reaction aliquots in an acid suspension (HCl, pH = 2.0−2.5) of activated charcoal. Because **3A** and **3B** (Figure 2) rapidly degrade in acid, their formation can be detected prior to release from the enzyme, thereby allowing the determination of kinetic constants up to and including the formation of **3A** and **3B** as a part of the pre-steady-state rate. The enzyme concentration, DNA concentration, and cofactor concentration are specific for each assay and are described in the figure legends. All reactions were saturated with the cofactor. The reaction buffer was 100 mM Tris-HCl (pH, 8.0), 10 mM EDTA, 10 mM DTT, and 0.5 mg/mL BSA.

Data Analysis. All reaction rates were calculated using Microcal Origin 5.0. All rates were reported as the best fit values ± standard deviation. The burst profiles were fit to a two-step irreversible mechanism (*27*):

$$[P](t) = \alpha E_t(1 - e^{-k_{pss}t}) + E_t k_{ss} t \qquad (1)$$

where [P](t) is the product concentration generated at time t, E_t is the total enzyme concentration, α is the factor that correlates stoichiometry between burst amplitude and enzyme concentration, k_{pss} and k_{ss} are pre-steady-state and steady-state rates, respectively, and t is the time from the start of the reaction. Unless otherwise indicated, all other profiles were analyzed using a linear equation. Each experiment was repeated in several independent measurements until the reproducibility of observed phenomena was established. The presented data show representative examples of analyzed phenomena.

pH Measurements. pH measurements between 6.5 and 7.5 were measured in 100 mM Bis-Tris-HCl (pK_a = 6.5 at 25°C), EDTA (10 mM), DTT (10 mM), and BSA (0.5 mg/mL). The pH profiles between 7.5 and 9.0 were measured in 100 mM Tris-HCl (pK_a = 8.1 at 25°C), EDTA (10 mM), DTT (10 mM), and BSA (0.5 mg/mL). The catalytic rates were within 10% when measured in Bis-Tris and Tris at pH 7.5. The pH profiles were analyzed using a single acidic and basic site (*28*):

$$v = \frac{V_{max}}{1 + 10^{-pH}/K_1 + K_2/10^{-pH}} \qquad (2)$$

where V_{max} is the maximal rate observed in the pH profile, K_1 is the acidic constant, and K_2 is the basic constant. The expected SKIE at the given pH and pK_a for the active site cysteine was calculated using the relations (*29*):

$$10^{pH-pK_a} = [cys\text{-}]/[Hcys]$$

and

$$2 = \frac{[\text{cys}_D\text{-}]/[\text{Dcys}]}{[\text{cys}_H\text{-}]/[\text{Hcys}]} \quad (3)$$

where [cys-] is the concentration of unprotonated cysteine, [cys_D-] and [cys_H-] are the concentrations of unprotonated cysteine in D_2O and H_2O buffer, [Dcys] and [Hcys] are the concentrations of protonated cysteine in D_2O and H_2O buffer, and the ratio of unprotonated and protonated cysteine in D_2O is two times higher than the ratio of unprotonated and protonated cysteine in H_2O. The sum of [cys_D-] and [Dcys] or [cys_H-] and [Hcys] equals the total cysteine concentration.

SKIE Measurements. All experiments in D_2O buffers were measured in parallel with corresponding H_2O experiments, and except for the solvent difference the two reactions are identical. The D_2O buffer was prepared as 10×, and its pH was adjusted, taking into account the pD vs pH correction (*29*) to be the same as in the corresponding H_2O buffer. Proton inventory profiles were analyzed using different forms of the Gross−Buttler equation (*29*):

$$k_\nu^{D_2O} = k^{H_2O}\frac{(1 + \nu - \nu\phi^T)^n}{(1 + \nu - \nu\phi^G)^m}Z^{-\nu} \quad (4)$$

where $k_\nu^{D_2O}$ is the measured rate at the given fraction of D_2O, k^{H_2O} is the rate measured in 100% H_2O, ν is the fraction of D_2O at which the rate was measured (i.e., 0.1, 0.2, 0.3, etc.), ϕ_T and ϕ_G are deuterium fractionation factors at the transition and the ground state, respectively, and Z is a cumulative fractionation factor for multiple small sites (*29*). Different forms of eq 4 can be produced by changing the values for parameters n, m, and Z as described in the Results section. Each form of eq 4 represents a unique mechanism with a distinct shape. Accordingly, each proton inventory profile was analyzed using several forms of eq 4, and the best fits were chosen on the basis of error in the best fit parameters, random distribution of the best fit residuals, and resolution between the fit parameters.

RESULTS

Methylation and Proton Exchange Reactions with ^{3}H-Poly-(dG-dC) (Figure 4). We measured the proton exchange rates in the presence of AdoMet and AdoMet analogues and in the absence of cofactors to focus on the catalytic events involving the cytosine C^5 (Figure 2, conversions **2** → **3A** or **2** → **3B**). The experiments were inspired by previous studies which showed that the cofactor can modulate the exchange (*17*) and cytosine deamination rates (*21*−*23*). The AdoMet analogues used in this study differ only at the position of the active methyl group (Figure 3). The exchange rates vary by over 3 orders of magnitude when measured in the presence of different cofactor analogues or in the absence of the cofactor (Table 1). The exchange rates are low in the presence of AdoMet (Figure 4A) and AdoHcy, intermediate with *N*-methyl-AdoMet, and high with sinefungin and in the absence of the cofactor (Figure 4B, Table 1). The relatively high tritium release rates in the presence of AdoMet result from the methylation reaction (Figure 2, **3A** → **4A**); thus no net exchange occurs with AdoMet (Figure 2, **3B** → **4B**). A stoichiometric proton release during the steady-state methylation reaction was shown before (*17*). Here we show that the methylation and proton release reactions have identical pre-steady-state rates. Thus, in the presence of AdoMet, intermediate **2** leads exclusively to methyl transfer (Figure 2, **2** → **3A**). A pre-steady-state burst is observed during AdoMet-dependent methylation and exchange (Figure 4A), in the exchange reaction in the presence of sinefungin (Figure 4B), and in the ^{3}H exchange reaction without cofactors (Figure 4B). The relatively large errors for the reported pre-steady-state rates (Table 1) are caused by the fast rates, allowing only for measurements of the burst and later stages of the reaction (Figure 4B). The pre-steady-state burst in the methylation reaction indicates that the steps leading to methyl transfer (Figure 2, **2** → **3A**) are faster than the subsequent steps, while the pre-steady-state burst in the exchange reaction indicates that the proton transfer (Figure 2, **2** → **3B**) at C^5 is faster than the subsequent steps. In summary, this study shows that the ability of different cofactor analogues to support or inhibit the exchange rates is dependent on the availability of a proton proximal to the C^5 moiety of the target cytosine (Figure 3).

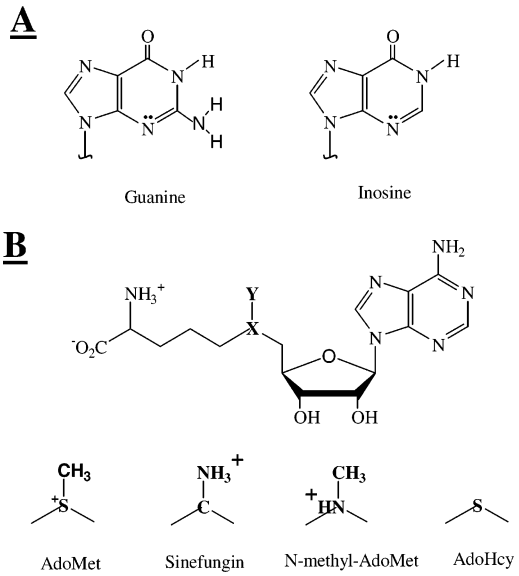

FIGURE 3: Structures of inosine and guanine (A) and AdoMet and its analogues (B).

Table 1: Pre-Steady-State and Steady-State Rate Constants for Methylation and ^{3}H Exchange Reactions[a]

	poly(dG-dC)		poly(dI-dC)[b]
	pss	ss	ss
wild type			
methylation (AdoMet)	140 ± 20	40 ± 4	65 ± 8
exchange (AdoMet)	146 ± 15	43 ± 4	230 ± 25
exchange (sinefungin)	500 ± 200	44 ± 3	165 ± 20
exchange (no cofactor)	650 ± 200	105 ± 10	10 ± 1
exchange (N-AdoMet)	33 ± 5	33 ± 5	145 ± 15
exchange (AdoHcy)	0.1 ± 0.02	NM	0.5 ± 0.005
$Gln^{237}Trp$			
methylation (AdoMet)	1.10 ± 0.05	NM	1.15 ± 0.1
exchange (AdoMet)	1.06 ± 0.04	NM	1.15 ± 0.05
exchange (no cofactor)	0.045 ± 0.008	NM	0.047 ± 0.006
exchange (sinefungin)	0.31 ± 0.02	NM	NM
exchange (N-AdoMet)	0.23 ± 0.03	NM	NM

[a] All rates are expressed as h^{-1} ± best fit error. NM, not measured. All values below the $Gln^{237}Trp$ row are for this mutant. [b] The reactions with poly(dI-dC) do not show a pre-steady-state (pss) burst, so the rates measured during the first turnover and the subsequent turnovers are all indicated as the steady-state (ss) rates.

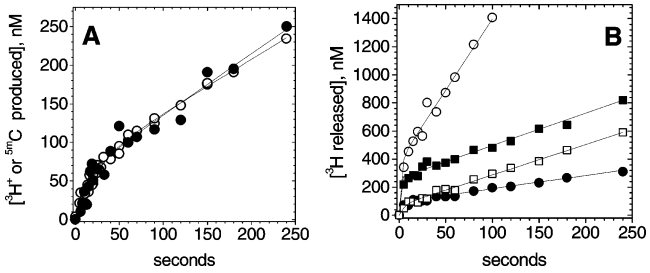

FIGURE 4: ^{3}H exchange and methylation reaction with ^{3}H-poly-(dG-dC). (A) ^{3}H exchange (○) and methylation rates (●) were measured in parallel by using M.HhaI (75 nM), ^{3}H-poly(dG-dC) (10 μM bp, 80 cpm/pmol), and ^{14}C-AdoMet (12 μM, 130 cpm/pmol). The rates were calculated using eq 1. (B) All reactions were measured in the presence of M.HhaI (285 nM) and ^{3}H-poly(dG-dC) (8 μM bp, 88 cpm/pmol). The reactions with sinefungin (10 μM) at pH = 8.0 (■) and pH = 6.5 (●) are shown. The reactions in the absence of the cofactor at pH = 8.0 (○) and pH = 6.5 (□) are also shown.

Analysis of pH and Solvent Kinetic Isotope Effects (SKIE) during Methylation and Exchange Reactions with Poly(dG-dC) (Figure 5). Previous studies suggested that nucleophilic attack by the active site Cys^{81} is rate limiting during methylation (*10*, *18*). Because cysteine has a unique 2-fold preference for hydrogen vs deuterium (*29*), pH/SKIE studies can be used to probe if the rate-limiting step in methylation or any of the exchange reactions depends on nucleophilic attack by Cys^{81} (*30*−*33*). If Cys^{81} attacks the target base as the thiolate, the observed reactions will give an inverse SKIE with the ground state ϕ_G close to 0.5 (eq 4 and ref *29*). If Cys^{81} attacks as the thiol and is deprotonated during nucleophilic attack, the reaction will give a normal SKIE and the transition state ϕ_T will be close to 0.5 (eq 4 and ref *29*). Both effects should disappear as the pH increases above the pK_a for the active site cysteine. We measured the pH profiles for the pre-steady-state rates during methylation and different exchange reactions (e.g., in the absence of cofactors and in the presence of sinefungin) to determine the number of pH-sensitive steps and the corresponding pK_a values (Figure 5). In reactions without cofactor analogues and with sinefungin we show that changes in pH affect the intercept in the pre-steady-state burst (Figure 4B), since the pre-steady-state rates were too fast to allow accurate determination of the kinetic constants. The pH profiles were analyzed using eq 2 and can be best described assuming a single protonation site with pK_as ranging from 7.4 to 7.8 (Table 2). Interestingly, the pH profiles are similar even though the catalytic rates vary by 3 orders of magnitude, suggesting that a similar residue(s) is (are) critical for the pH-sensitive step. The observed SKIE is specific for each reaction and principally pH-independent, unlike the pH−activity profiles. Thus, the pH and SKIE profiles are at least in part caused by different groups, and it is thus unlikely that a single rate-limiting step is being probed by these methods. We used eq 3 to generate the predicted SKIE profiles for a reaction limited by a nucleophilic cysteine, the medium value for the measured pK_a range (Table 2), and the known fractionation factor for cysteine ϕ = 0.5 (*29*).

The exchange reaction without cofactor has an inverse SKIE, and the SKIE increases with increasing pH (Figure 5B). This pH-induced change in the SKIE indicates that the SKIE is at least in part a result of a pH-sensitive step. If the pH response is controlled by the active site Cys^{81}, a pH-induced change in the SKIE suggests that conversion between intermediates **1** and **2** contributes to the rate-determining step. The observed pH/SKIE profiles are different from the pH/SKIE profiles expected for a reaction that is *primarily* controlled by a cysteine nucleophilic attack with the measured pK_a (Figure 5B, upper panel). However, the observed SKIE may be caused by the nucleophilic cysteine and some other group, which is consistent with dome-shaped proton inventory studies (Figure 10A).

Methylation and Tritium Exchange Reaction with Poly-(dI-dC) and AdoMet Analogues (Figures 6 and 7). We

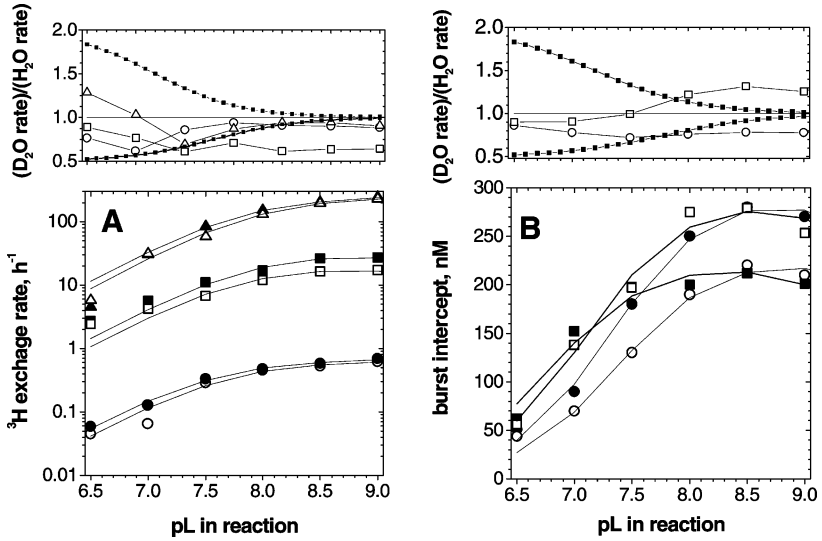

FIGURE 5: pH profiles and SKIE analysis of the ^{3}H exchange reaction with ^{3}H-poly(dG-dC). (A) pH profile for the ^{3}H exchange reaction with AdoMet (▲, △), *N*-methyl-AdoMet (■, □), and AdoHcy (●, ○) in H_2O and D_2O, respectively. Each profile was analyzed using eq 2, and the best fit values are listed in the Table 2. In the upper panel the symbols represent AdoMet (△), *N*-methyl-AdoMet (□), and AdoHcy (○). The dashed line is calculated using eq 3 and shows the expected SKIE if the rate-limiting step is primarily dependent on a nucleophilic cysteine with pK_a = 7.5. (B) pH profile for the burst intercept in the ^{3}H exchange reaction with sinefungin (●, ○) and in the absence of the cofactors (■, □) in H_2O and D_2O. Each profile was analyzed using eq 2, and the best fit values are listed in Table 2. In the upper panel the symbols represent sinefungin (○) and the reaction in the absence of the cofactor (□). The dashed line is calculated using eq 3 and represents the expected SKIE if the rate-limiting step is primarily dependent on a nucleophilic cysteine with pK_a = 7.5.

Table 2: Summary of the pH and SKIE Analysis of the Presented Reactions

	apo	sinefungin	AdoMet	N-AdoMet	AdoHcy
			Wild Type with ^{3}H-Poly(dG-dC) Substrate		
SKIE type and shape[a]	inverse and dome shape	normal and bowl shape	none	normal and dome shape	none
ϕ_T	3.2 ± 1	0.42 ± 0.07		0.34 ± 0.04	
ϕ_G	2.1 ± 0.7	1.8 ± 0.2		1.4 ± 0.2	
pK_a(H_2O)	7.7 ± 0.08	7.3 ± 0.05	7.8 ± 0.06	7.8 ± 0.2	7.5 ± 0.07
pK_a(D_2O)	7.1 ± 0.08	7.3 ± 0.07	7.9 ± 0.04	7.4 ± 0.3	7.6 ± 0.1
comments				$Z = 1 \pm 0.03$	
			Wild Type with ^{3}H-Poly(dI-dC) Substrate		
SKIE type and shape[a]	inverse and almost linear	normal and bowl shape	normal and linear when reciprocal	normal and linear when reciprocal	none
ϕ_T	3.7 ± 0.5	0.47 ± 0.05	1.08 ± 0.32	0.94 ± 0.33	NM[b]
ϕ_G	1.1 ± 0.2	1.7 ± 0.12	2.04 ± 0.66	2.15 ± 0.7	NM[b]
pK_a(H_2O)		7.4 ± 0.07	7.6 ± 0.04	7.5 ± 0.08	7.6 ± 0.06
pK_a(D_2O)		7.5 ± 0.05	7.4 ± 0.06	7.7 ± 0.07	7.5 ± 0.08
comments	no pH response	slower than GC in pss[c] and faster in ss[c]	exchange faster than methylation	5 times faster with IC relative to GC	5 times faster with IC relative to GC
			Gln^{237}Trp with ^{3}H-Poly(dG-dC) Substrate		
SKIE type and shape[a]	inverse and mild dome shape	normal and linear when reciprocal	inverse and mild dome shape	inverse and mild dome shape	
ϕ_T	2.4 ± 0.5	1.1 ± 0.3	2.2 ± 0.8	1.8 ± 0.04	
ϕ_G	1 ± 0.5	2.1 ± 0.6	1.1 ± 0.4	0.96 ± 0.2	
pK_a(H_2O)	NM[b]	7.3 ± 0.06	7.4 ± 0.12	7.4 ± 0.07	
pK_a(D_2O)		7.5 ± 0.1	7.5 ± 0.1	7.6 ± 0.1	
comments		SKIE type and shape changes with pH	SKIE changes with the pH	SKIE type and shape changes with pH	

[a] To describe the shape, we used the nomenclature described in ref *29*; inverse means the reaction is faster in D_2O, and normal means the reaction is slower in D_2O. [b] NM, not measured. [c] pss stands for pre steady state; ss stands for steady state.

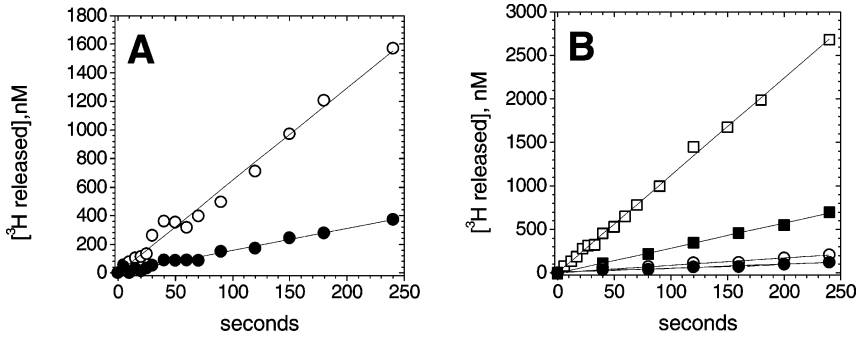

FIGURE 6: ^{3}H exchange and methylation reaction of ^{3}H-poly(dI-dC). (A) ^{3}H exchange (○) and methylation rates (●) were measured in parallel using M.HhaI (100 nM), ^{3}H-poly(dI-dC) (10 μM bp, 13 cpm/pmol), and ^{14}C-AdoMet (12 μM, 130 cpm/pmol). The rates were calculated by linear regression. (B) ^{3}H exchange reaction with sinefungin (□, ■) and in the absence of the cofactor (○, ●) at pH = 8.0 and 6.5, respectively. All reactions with ^{3}H-poly(dI-dC) were analyzed using linear equations.

compared the methylation and proton exchange reactions with ^{3}H-poly(dG-dC) and ^{3}H-poly(dI-dC) to understand how enzyme−DNA interactions alter catalysis. Poly(dI-dC) is a good substrate for the methylation and exchange reactions (Table 1 and Figure 6). Except for the exchange reaction in the absence of the cofactor (Table 1), the rate for poly(dI-dC) and the pre-steady-state and steady-state rate for poly(dG-dC) are quite similar. The reaction with poly(dI-dC) is slightly faster with AdoHcy and *N*-methyl-AdoMet and slightly slower with sinefungin (Table 1). The AdoMet-dependent methylation reaction and the sinefungin-dependent exchange reactions have 2-fold slower rates with poly(dI-dC), but the steady-state rates are 4-fold faster than with poly(dG-dC) (Table 1). We observe no burst with poly(dI-dC) during methylation (Figure 4A vs Figure 6A), nor in the exchange reactions with sinefungin (Figure 4B vs Figure 6B), indicating that the product release steps are faster and thus no longer rate limiting. Surprisingly, AdoMet-dependent methylation with poly(dI-dC) shows exchange rates which are four times faster than the methylation rates (Figure 6A and Table 1). The excess tritium released in the methylation reaction during the first turnover indicates that proton transfer at cytosine C^5 (Figure 2, **2** → **3B**) occurs prior to methyl transfer (Figure 2, **2** → **3A**). In addition, since a single target base attack can result in only one tritium release (Figure 2, **2** → **3B** → **4B**), the excess tritium released during the multiple catalytic turnovers in the methylation reaction indicates that the enzyme rapidly attacks and releases several target bases before catalyzing methyl transfer from the bound AdoMet. Such a rapid interchange between different bases indicates that there is a dynamic equilibrium between intermediates **1** and **2** (i.e., Figure 2, **1** ↔ **2**) and that the base restacking is fast and in a direct competition with the covalent adduct formation (**1** → **2**, Figure 2) and methyl transfer (**2** → **3A**, Figure 2). Crystallographic studies (*34*), ^{19}F NMR studies (*15*), and fluorescent studies (*14*) showed

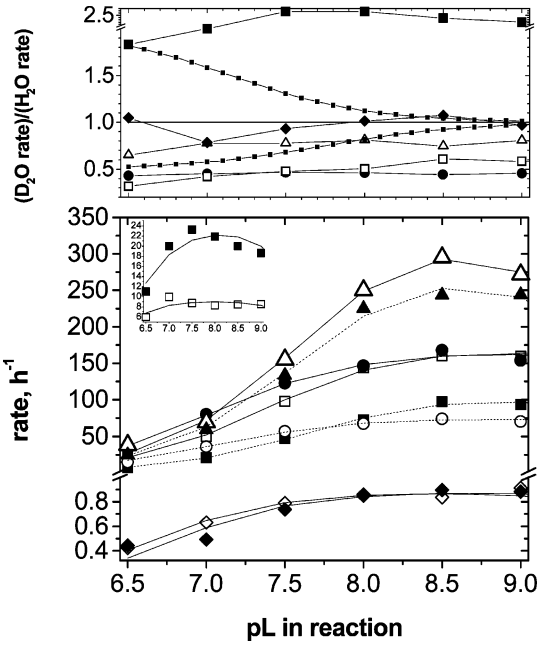

FIGURE 7: pH profile and SKIE analysis of the ^{3}H exchange reaction with ^{3}H-poly(dI-dC). The pH profiles for the ^{3}H exchange reaction with AdoMet (▲, △), sinefungin (●, ○), *N*-methyl-AdoMet (□, ■), and AdoHcy (◆, ◇) in H_2O and D_2O, respectively, are shown. The insert shows the pH profile for the reaction without cofactors (■, □) in D_2O and H_2O, respectively. All profiles were analyzed using eq 2, and the best fit values are listed in the Table 2. The upper panel shows the ratios between the rates measured in D_2O and H_2O in the presence of AdoMet (○), sinefungin (●), *N*-methyl-AdoMet (□), AdoHcy (△), and apoenzyme (■). The dashed lines are calculated using eq 3 and show the expected SKIE if the rate-limiting step is primarily dependent on a nucleophilic cysteine with pK_a = 7.5 as described in the text.

that the extrahelical base can exist as a stable and distinct intermediate. Our results show that with poly(dI-dC) the extrahelical base is a short-lived intermediate. Our observation that the exchange rate is much faster with poly(dI-dC) than methylation supports the idea that the methyl transfer step is limiting.

The pH profiles (Figure 7) for the exchange reaction with AdoMet and poly(dI-dC) and different analogues are very similar and closely resemble the profiles in similar reactions with poly(dG-dC) (Table 2 and Figure 5). Thus, any differences between poly(dG-dC) and poly(dI-dC) do not affect the pH-sensitive step. The SKIE for each reaction with poly(dI-dC) is unique and pH-independent. Thus, as with poly(dG-dC), the SKIE and pH profiles are at least in part caused by different phenomena. The most significant distinction between these two substrates is observed in the exchange reaction without cofactor (Figures 6B and 7, insert), with the poly(dI-dC) reaction being 2 orders of magnitude slower, is largely pH-independent, and has a large inverse SKIE. These observations suggest that in the absence of the cofactor the exchange reaction with poly(dI-dC) has a unique rate-limiting step and mechanism.

Processivity on Poly(dG-dC) and Poly(dI-dC) Substrates (Figure 8). To measure the processivity on DNA substrates, we prepared two identical exchange reactions, one containing only labeled DNA (called the *free* reaction) and one having ^{3}H-labeled DNA plus an *n*-fold excess (usually $n = 10$) of unlabeled DNA (called the *dilute* reaction). Both reactions are started simultaneously by adding equal amounts of enzyme. As expected, the ^{3}H release rate in the free reaction is *n*-fold higher than in the dilute reaction. By the end of the first turnover (Figure 8, arrow), an aliquot from the free reaction is mixed with an *n*-fold excess of unlabeled DNA (*chase* reaction). If the enzyme is fully processive, addition of the 10-fold excess of unlabeled substrate in the chase reaction will not affect the tritium release rates. If the enzyme is not processive, the ^{3}H release rates in the chase reaction will be immediately identical to the tritium release rates in the dilute reaction. A partially processive enzyme in which only a fraction of the enzyme molecules stay on the original substrate will result in the ^{3}H release rates in the chase reaction being between the tritium release rates for the free and dilute reactions. The rate will gradually decrease with each turnover until the chase and dilute reactions become

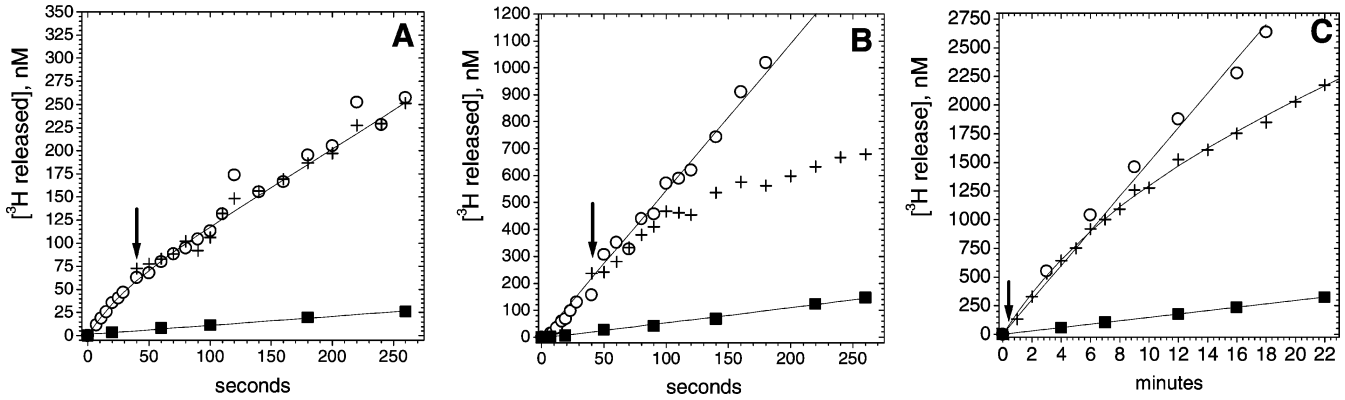

FIGURE 8: Chase processivity assay with M.HhaI and ^{3}H-poly(dG-dC) (A) or ^{3}H-poly(dI-dC) (B) and M.SssI with ^{3}H-poly(dI-dC) (C). (A) The free (○) reaction had M.HhaI (50 nM), ^{3}H-poly(dG-dC) (8 μM bp, 102 cpm/pmol), and AdoMet (10 μM). The dilute reaction (■) was prepared from a free reaction aliquot by adding a 10-fold excess of unlabeled poly(dG-dC). Free and dilute reactions were started simultaneously; the chase reaction (+) was started 40 s later (after the first turnover) by adding unlabeled poly(dG-dC) (80 μM bp) to the free reaction aliquot. (B) The free (○) reaction had M.HhaI (100 nM), AdoMet (10 μM), and ^{3}H-poly(dI-dC) (8 μM bp, 24 cpm/pmol). The dilute reaction (■) was prepared from a free reaction aliquot by adding a 10-fold excess of unlabeled poly(dI-dC). Free and dilute reactions were started simultaneously; the chase reaction (+) was started 45 s after the free reaction (after the second turnover) by adding unlabeled poly(dI-dC) (100 μM bp) to the free reaction aliquot. (C) The free (○) reaction had M.SssI (30 nM), ^{3}H-poly(dI-dC) (10 μM bp, 24 cpm/pmol), and AdoMet (10 μM). The dilute reaction (■) was prepared from a free reaction aliquot by adding a 10-fold excess of unlabeled poly(dI-dC). The chase reaction (+) was started 45 s after the free reaction by adding 100 μM bp unlabeled poly(dI-dC) to a free reaction aliquot.

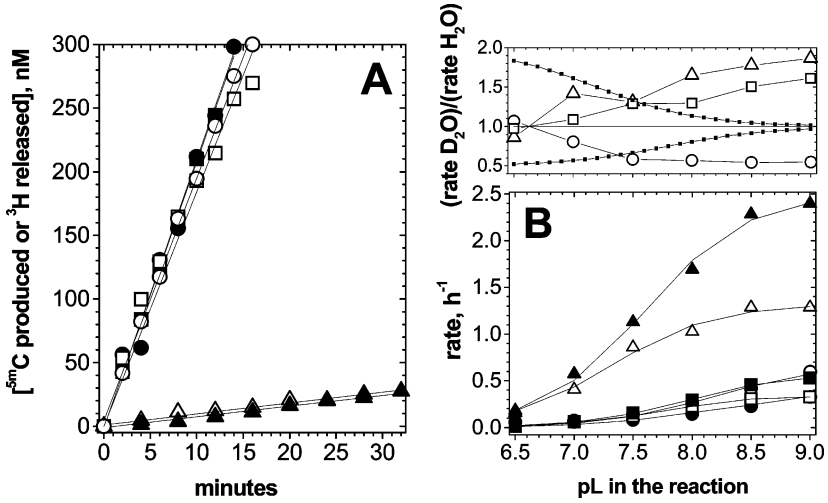

FIGURE 9: (A) Gln^{237}Trp mutant exchange and methylation reactions with ^{3}H-poly(dG-dC) and ^{3}H-poly(dI-dC) and (B) pH/SKIE profiles in the reaction with ^{3}H-poly(dG-dC). (A) Methylation and the ^{3}H exchange rates with the Gln^{237}Trp mutant (1000 nM) were measured in parallel using ^{14}C-AdoMet (12 μM, 131 cpm/pmol) and ^{3}H-poly(dG-dC) (12 μM bp, 88 cpm/pmol) or ^{3}H-poly(dI-dC) (12 μM bp, 25 cpm/pmol). The symbols represent the ^{3}H exchange (○, □) and methylation (●, ■) reaction with ^{3}H-poly(dG-dC) and ^{3}H-poly(dI-dC), respectively, and the ^{3}H exchange reaction without cofactor and ^{3}H-poly(dG-dC) (▲) and ^{3}H-poly(dI-dC) (△). All profiles were analyzed using a linear equation, and the best fit values are listed in the Table 1. (B) The lower panel shows pH profiles for exchange reactions measured with AdoMet (▲, △), sinefungin (○, ●), and *N*-methyl-AdoMet (■, □) in D_2O and H_2O, respectively. The pH profiles were analyzed using eq 2, and the best fit values are given in Table 2. The upper panel shows the ratios between the rates measured in D_2O and H_2O in the presence of AdoMet (△), sinefungin (●), and *N*-methyl-AdoMet (□) in D_2O and H_2O, respectively. The dashed lines are calculated according to eq 3 and represent the expected SKIE for a reaction that is primarily limited by cysteine nucleophilic attack with $pK_a = 7.5$ as described in the text.

identical. We find that M.HhaI is fully processive for five turnovers in the methylation reaction with poly(dG-dC) substrate. M.HhaI is only partially processive in the methylation reaction with the poly(dI-dC) substrate for about three to four turnovers. Since processivity experiments measure tritium release rates rather than the methyl transfer rates, the small processivity on poly(dI-dC) substrates can be attributed to excess tritium released during the methylation reaction with the poly(dI-dC) substrate (Figure 6A). A positive control was included in the form of M.SssI since this enzyme was previously shown to be processive (*35*). Here we show that M.SssI catalyzes 30 turnovers on the same DNA molecule.

Exchange Reaction with the Gln^{237}Trp Mutant (Figure 9). Gln^{237} interacts with the amino group on the C^2 of the orphan guanine; this interaction forms part of the network of hydrogen bonds that stabilize intermediates **1** and **2** (Figure 2 and ref *36*). The Gln^{237}Trp mutant is one of the least active Gln^{237} mutants (*19*). We were interested in using the kinetic analyses presented for the wild-type M.HhaI to identify which step(s) during catalysis is (are) significantly altered in the mutant. The Gln^{237}Trp mutant has methylation and exchange rates with poly(dG-dC) and poly(dI-dC) that are more than 10-fold slower than those of the wild-type enzyme (Table 1). The exchange rates are slowest in the absence of the cofactor, and there is little difference in catalytic rates with AdoMet, sinefungin, and *N*-methyl-AdoMet. Unlike the WT enzyme, we observe identical rates for the methylation and tritium release kinetics during AdoMet-dependent methylation of poly(dI-dC) (Figure 9A), and the mutant shows identical methylation and exchange kinetics for the two DNA substrates (Figure 9A).

The pH profiles with the mutant (Figure 9B) closely resemble the pH profiles in similar reactions with the WT enzyme (Figure 5 and Table 2). Since reactions with the mutant and the WT enzyme show very different rates, the observed similarity in the pH profiles further supports the idea that the ionization state of similar residues carries out similar functions in the two proteins. The mutant and the wild-type enzymes show distinct SKIE (Figures 5, 7, and 9B). For example, all reactions with the mutant show pH-dependent changes in the SKIE (Figure 9B); thus, the SKIE is at least in part caused by the pH-sensitive step.

Proton Inventory Experiments (Figure 10). Proton inventory profiles are measured at varying ratios of D_2O and H_2O (*29*). This approach represents a sensitive strategy to describe and compare the rate-limiting step in enzyme-catalyzed reactions (*29*). We measured proton inventories with the exchange reactions to determine if different reactions share similar intermediates and rate-limiting steps. For those reactions showing a pre-steady-state burst, the proton inventories were measured in the pre steady state; reactions showing linear profiles were measured in the first and subsequent turnovers. Proton inventories are usually described according to their shape and fractionation factors, i.e., ϕ_T and ϕ_G (*29*). The shape of the proton inventory profile indicates the number of steps or groups controlling the SKIE and whether the observed SKIE is caused in the ground state, transition state, or both (*29*). The fractionation factors can help to identify the group that causes the SKIE (i.e., $\phi = 0.5-0.6$ indicates cysteine) and also to compare proton inventory profiles from different reactions. The proton inventory profile is fit by using different forms of eq 4 involving different values and combinations of the *n*, *m*, and *Z* parameters. We used eq 4 to identify the simplest form that describes the proton inventory profiles based on the following options and parameters: (i) two SKIE-sensitive steps in the transition state ($n = 2$, $m = 0$, $Z = 1$); (ii) two SKIE-sensitive steps in the ground state ($n = 0$, $m = 2$, $Z = 1$); (iii) one SKIE-sensitive step in the ground state and one in the transition state ($\upsilon = 1$, $\upsilon = 1$, $Z = 1$). We also

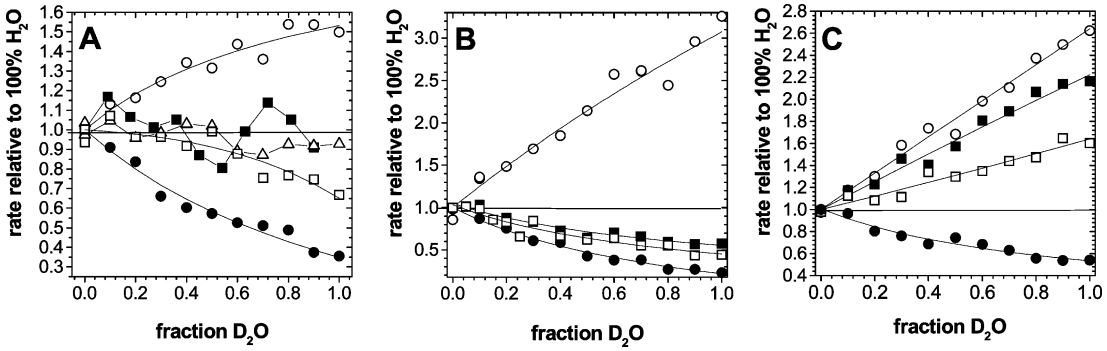

FIGURE 10: Proton inventory for the ^3H exchange reaction with (A) ^3H-poly(dG-dC), (B) ^3H-poly(dI-dC), and (C) the $Gln^{237}Trp$ mutant and ^3H-poly(dG-dC). In all three panels the symbols indicate proton inventory profiles for reaction without cofactors (○), AdoMet (■), *N*-methyl-AdoMet (□), and sinefungin (●). Panel A also has data for AdoHcy (△). The profiles represent rates measured in the pre steady state or in the steady state as described in the text. All profiles were analyzed using the Gross−Butler equation (eq 4), and the best fit values are given in the Table 2.

considered a situation involving contributions from multiple sites; i.e., the *Z* factor was allowed to float and $n = 1$, $m = 0$ or $n = 0$, $m = 1$. On the basis of the best fit residuals, the proton inventory profiles are best described as one SKIE-sensitive step in the transition state and one in the ground state (i.e., $n = 1$, $m = 1$, $Z = 1$). The calculated best fit fractionation factors are summarized in Table 2, and the best fit profiles are presented in Figure 10.

Different proton inventory profiles are observed during methylation with poly(dG-dC), methylation with poly(dI-dC), and methylation with the $Gln^{237}Trp$ mutant. Therefore, these reactions depend on different relative contributions from several steps, implicating distinct mechanisms. In contrast, the proton inventories and fractionation factors for the exchange reactions with sinefungin and poly(dG-dC) or poly(dI-dC) are within experimental error identical (Table 2), indicating that they have very similar mechanisms. All reactions with the wild-type enzyme have a ground state fractionation factor (ϕ_G) between 1.8 and 2, while the transition state fractionation factor ϕ_T is unique for each reaction (Table 2). The proton inventory analysis shows that the exchange reactions with both DNA substrates in the absence of cofactor are similar to the reactions catalyzed by the $Gln^{237}Trp$ mutant (Table 2): an inverse SKIE, an increase in SKIE with an increasing pH, and a transition state fractionation factor ϕ_T close to 2 (Table 2). The dome-shaped proton inventory profiles for the proton exchange reaction without cofactor (Figure 10A) suggest that the SKIE and multiple steps are rate limiting and determine the SKIE (*29*).

DISCUSSION

Despite a wealth of information regarding DNA cytosine methyltransferases, and in particular M.*Hha*I, there is little experimental evidence regarding three fundamental aspects of enzyme catalysis: the identity and roles of critical active site groups other than Cys^{81}, the identity and roles of reaction intermediates, and the rate constants associated with their interconversion (Figure 2). Our goals were to (1) understand which steps are rate limiting (Figure 2), (2) characterize the relative stabilities of intermediates **1** and **2**, (3) characterize the interconversion kinetics involving intermediates **1** and **2**, (4) investigate the extent to which solvent molecules gain access to intermediate **2**, and (5) characterize how protein−DNA interactions alter the stability of intermediates **1** and **2**. Our approach uses both base and cofactor analogues (Figure 3) in conjunction with several kinetic strategies.

Stabilization of the extrahelical cytosine (base flipping, Figure 1) within the enzyme's active site (Figure 2, intermediate **1**) has been proposed to activate the ring for nucleophilic attack at the C^6 position by protonation at N^3 (Figure 2, **1**, and refs *18* and *37*). Nucleophilic attack to form the covalent intermediate (Figure 2, **2**) is an essential feature of all DNA cytosine methyltransferases, including the enzymes involved in epigenetic regulation in humans (*38*). Indeed, nucleophilic attack at the pyrimidine C^6 position is core to all C^5 pyrimidine methyltransferases and the basis of drug action for several clinically used mechanism-based cancer treatments (*5*, *39*). Formation of intermediate **2** disrupts the aromaticity of the pyrimidine, while the insertion of electron density deriving from the thiolate enables the normally unreactive pyrimidine to attack a proximal electrophile. Experiments demonstrating that M.HhaI catalyzes the exchange of tritium placed at the cytosine C^5 position provided the first definitive evidence for the formation of intermediate **2** (*17*). This cytosine C^5 exchange reaction provides a unique opportunity to expand our ability to analyze the target base attack beyond the limitations of routine methylation assays. Like methylation, the exchange reaction requires that the enzyme forms a covalent adduct with the target base. Both reactions are the result of electrophilic addition at the cytosine C^5, and both reactions end with the β elimination involving proton removal at the cytosine C^5 position (Figure 2, **3A** → **4A** and **3B** → **4B**).

In this study we find that the tritium exchange rates vary by 3 orders of magnitude when measured in the presence of different cofactor analogues or in the absence of the cofactor (Table 1). The AdoMet analogues used in this study differ only at the position of active methyl group (Figure 3), and the analogues' ability to support the exchange reaction correlates with the proton presence at the position of the active methyl group (Figure 3). Possible mechanisms by which AdoMet and AdoHcy can inhibit the exchange reaction were previously described (*17*, *20*, *40*). Briefly, AdoMet and AdoHcy can inhibit the exchange reaction (i) by controlling the stereochemistry of the β elimination step (Figure 2, **3B** → **4B**), (ii) by affecting the enzyme's ability to form intermediates **1** or **2**, or (iii) by affecting proton access at the C^5 of the activated target base (Figure 2, **2** →

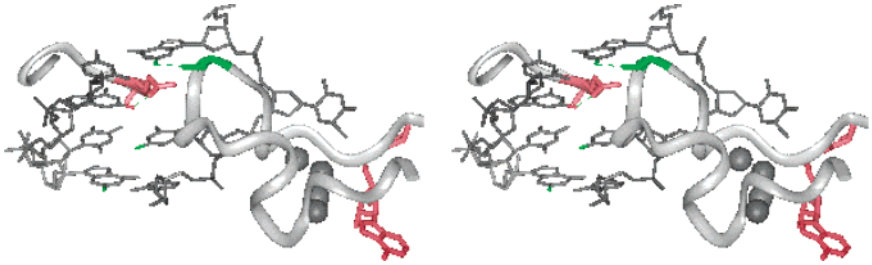

FIGURE 11: Structure of the active site loop, the Gln^{237} site, and the GCGC recognition sequence with an extrahelical base (*7*). DNA is shown in thin gray lines. The gray ribbon in the front represents the active site loop (amino acids 80−99) in the closed position when Ile^{86} (green) can make a hydrogen bound with the C^2 amino group (green) on guanine that is in the 5′ position relative to target cytosine. The background gray ribbon represents the peptide backbone with Gln^{237} (red) which makes a hydrogen bond with the C^2 amino group (red) on the orphan guanine. The cofactor is shown in red in the lower right corner, while the four solvent molecules near the target base are shown as gray spheres. The C^2 amino groups (green) on two of guanine residues are exposed to solvent and make no contacts with enzyme.

3B). Our exchange assay detects tritium exchange upon delivery of the proton to the cytosine C^5 position (Figure 2, **3A**) and the pre-steady-state rates do not depend on the stereochemistry of proton release (Figure 2, **3B** → **4B**). Thus, stereochemical control of the proton release step by the different analogues seems unlikely. It is equally unlikely that the analogues interfere with enzyme's ability to form intermediates **1** and **2** because (i) we observe different exchange rates with poly(dG-dC) and poly(dI-dC) in the presence of AdoMet (Figures 4A and 6A), (ii) AdoMet does not support the exchange reaction with poly(dG-dC) (Figure 4A), (iii) our pH/SKIE studies (Figures 5 and 8) are inconsistent with a rate-limiting step involving nucleophilic attack by Cys^{81}, and (iv) the subtle structural differences within the different cofactor analogues would seem unlikely to cause such dramatic changes in the enzyme's ability to form intermediate **2**, since high exchange rates in the absence of any cofactor involving well-studied and large conformational changes in the enzyme (*7*) have minimal effects on the exchange process.

The observed pattern in modulation of the exchange rates by AdoMet analogues and the crystal structures of M.HhaI (*7*, *40*, *41*) suggest that the exchange rates depend on the proton access to the C^5 of the target base. The four analogues (Figure 3) are likely to bind the active site in the same fashion since the cocrystal structures of the two most diverse forms involving AdoMet (*41*) and AdoHcy (*7*) reveal similar cofactor binding orientations. We suggest that the most likely candidate for the proton donor is the cofactor and/or the solvent molecules that are frequently observed in the active site (Figure 11 and ref *42*). The high exchange rates in the absence of the cofactor can be attributed to solvent which has ready access to the C^5 on the activated target base [pK_a = 18 (*18*)]. The low exchange rates in the presence of AdoMet and AdoHcy are to be expected since their proximity to the cytosine C^5 (*7*, *18*, *40*) can block solvent access. Although sinefungin and *N*-methyl-AdoMet can also block solvent access to the cytosine C^5 position, the relatively high exchange rates may derive from the proximal amino groups found within these analogues. The exchange rates are higher with sinefungin than *N*-methyl-AdoMet, since sinefungin's three protons are most likely closer to the cytosine C^5.

In summary, our study of AdoMet analogues and the exchange reaction extends the previous study (*17*) which showed that AdoMet and AdoHcy inhibit the exchange reaction when compared to the same reaction without cofactors. We show that the ability of the cofactors to support the exchange reaction correlates with the proton access and proximity (Figure 3) at the C^5 on the target base. These insights allow us to describe the catalytic events following the formation of the covalent intermediate **2** (Figure 2, **2** → **3A** → **4A** and **2** → **3B** → **4B**) and the rate limiting step as described further in the text. Furthermore, the exchange reaction shows a similar cofactor dependency as was previously reported for the mutagenic deamination reaction (*23*). The similar trends are reasonable since C^5 protonation is known to increase deamination rates by at least 4 orders of magnitude (*37*). Because the deamination reaction is difficult to study mechanistically, the exchange reaction provides a convenient mechanistic probe of the common features of these reactions. For example, the exchange reaction could be used to investigate the extent to which eukaryotic cytosine methyltransferases (e.g., Dnmt1) support the deamination reaction[2] or to investigate the basis for any differences in the deamination kinetics observed with different bacterial enzymes (*22*).

pH/SKIE Studies. We used pH and SKIE studies (Figures 5 and 7) to probe if the rate-limiting step in methylation or any of the exchange reactions depends on nucleophilic attack by Cys^{81} involving the transition between intermediates **1** and **2** (Figure 2). Based on theoretical studies (*18*), nucleophilic attack by Cys^{81} is thought to be rate limiting during methylation (*10*, *42*). Our pH/SKIE analysis showed no evidence that the cysteine nucleophilic attack is rate limiting during methylation or any of the exchange reactions in the presence of the cofactor. Interestingly, we find that even though the relative exchange rates vary by orders of magnitude (Table 1), all exchange reactions have very similar pH profiles (Table 2), and in the majority of the reactions the SKIE (ratio between the rates measured in D_2O and H_2O) is pH-independent and unique for each reaction (Figures 5 and 7). To understand how the conversion between intermediates **1** and **2** (Figure 2) might affect catalytic rates, it is necessary to realize that this conversion is in principle reversible and that reversion back to intermediate **1** is expected if methyl transfer (**2** → **3A**) or proton transfer (**2** → **3B**) is relatively slow. If the rate of reversal (**2** → **1**) is at least severalfold faster than the specific catalytic process at cytosine C^5, intermediates **1** and **2** will be in equilibrium (i.e., Figure 2, **1** → **2**, and Figure 1). Several experimental observations support a rapid equilibrium between intermediates **1** and **2**. First we observe an excess release of tritium

[2] Ž. M. Svedružić and N. O. Reich, manuscript in preparation.

during the methylation reaction involving poly(dI-dC) (Figure 6A). Second, the pre-steady-state exchange kinetics with sinefungin and poly(dG-dC) (Table 1) show that the conversion between intermediates **1** and **2** can be severalfold faster than the subsequent methyl transfer step. Finally, the results of the pH/SKIE studies (Figures 5 and 7) are also compatible with the rapid equilibrium proposal. A decrease in pH results in protonation of Cys^{81} and a shift in the equilibrium between **1** and **2** in favor of intermediate **1**, which leads to a decrease in the catalytic rates. We observe that solvent changes (e.g., replacement of H_2O with D_2O) have little effect on the pK_a of Cys^{81} (*43*) but do affect hydrogen-bonding interactions and proton transfer steps that lead to the exchange reaction. Hence, pH/SKIE studies (Figures 5 and 7) reveal that a change in the pH does affect catalytic rates, while the SKIE is pH-independent and specific for the particular mechanism of the proton transfer at the C^5 on the target base. In summary, the most important consequence of our proposed rapid equilibrium mechanism is that the catalytic rates are dependent on the steps that control the concentration of intermediate **2** *and* the steps that control the conversion to intermediate **3A** (Figure 2, **2** → **3A**) or **3B** (Figure 2, **2** → **3B**); this is in contrast to the circumstance in which only the formation of intermediate **2** is rate limiting (Figure 2, **1** → **2**).

The exchange reaction in the absence of the cofactor is unique in several features. High exchange rates without cofactors in the presence of poly(dG-dC) (Figure 4B and ref *17*) indicate that conformational changes associated with the cofactor binding are not necessary for a successful target base attack (Table 1). An increased SKIE with increasing pH suggests that nucleophilic attack by Cys^{81} (Figure 2, **1** → **2**, and Figure 5) is at least partially rate limiting in the exchange reaction. Once intermediate **2** is formed, the proton transfer to cytosine C^5 is likely to be relatively efficient since the target base is fully accessible to solvent molecules in the absence of bound cofactor (Figure 11 and ref *42*). Thus, it appears unlikely that intermediates **1** and **2** are in rapid equilibrium in the absence of cofactor and that proton transfer at cytosine C^5 is rate limiting. Further support for these conclusions is presented below in the exchange reaction with poly(dI-dC), in our studies with the Gln^{237}Trp mutant and in the analysis of various M.HhaI structures. The cofactor binding increases the enzyme's affinity for DNA by orders of magnitude (*9*). Cofactor binding is believed to induce active site loop movement (amino acids 80−99 (*7*)) and extensive conformational changes in protein structure (*7*).

Methylation and Exchange with Poly(dI-dC). Crystallographic studies with different DNA sequences (*8*), theoretical analysis (*36*), and various M.HhaI mutants (*10*, *19*, *44*) suggest how M.HhaI:DNA interactions can affect DNA binding, target sequence recognition, and the base flipping process. Investigation of various proposed mechanisms requires suitable assays, and we sought to apply our exchange assays to this end. Poly(dI-dC) has several unique features that provide an opportunity to probe the importance of the active site loop (residues 80−99, Figure 11, and ref *7*), the base flipping mechanism, and the functional distinctions between M.HhaI and the more complex mammalian enzyme Dnmt1.[2] Poly(dI-dC) cannot form a hydrogen bond with Ile^{86} within the active site loop. Closure of this loop appears to be crucial for the stabilization of the extrahelical base (Figure 11 and ref *7*); however, its dynamics and precise function cannot be completely understood from the static crystal structures. Poly(dI-dC) is a unique probe for interactions between the active site loop and Ile^{86} since the hydrogen bond is between the C^2 amino group on guanine and the protein backbone (Figure 11 and ref *7*). We also used poly(dI-dC) as a probe of the interactions that may contribute to the base flipping process since, in contrast to the G·C pair, the I·C base pair has only two hydrogen bonds (Figure 3 and ref *45*). Finally, the studies with poly(dI-dC) provide a basis for investigating the mammalian enzyme, Dnmt1, which has a strong preference for poly(dI-dC) (*26*).[2]

Poly(dG-dC) and poly(dI-dC) substrates show similar methylation and exchange rates (Table 1), and methylation rates with poly(dG-dC) and poly(dI-dC) are similar to the catalytic rates previously reported with different DNA substrates (*9*, *10*, *17*, *44*). The similar catalytic rates (Table 1) indicate that any structural differences between poly(dG-dC) and poly(dI-dC), or other DNA substrates used in the past, have negligible impacts on the enzyme's ability to form intermediates **3A** and **3B** (Figure 2, **1** → **2** → **3A** or **1** → **2** → **3B**). This is consistent with the available structures of M.HhaI complexed to DNA, which show that the majority of the M.HhaI·DNA interactions involve the phosphate backbone (ref *7* and Figure 11) and numerous base contacts involve the major groove. Poly(dG-dC) and poly(dI-dC) have identical functional groups in the major groove (Figure 3), and the I·C and G·C base pairs share the same conformation (*45*).

The poly(dI-dC) substrate revealed insightful changes in the stability of intermediates **1** and **2** (Figures 4A and 6A), in the partitioning of intermediate **2** toward proton or methyl transfer (Figures 4A and 6A), and in catalytic processivity (Figure 8A,B). The main difference between poly(dG-dC) and poly(dI-dC) is in the potential hydrogen-bonding interactions involving Gln^{237} or Ile^{86} (ref *7* and Figure 11). The hydrogen bonds involving Gln^{237} and Ile^{86} are most likely important for different steps in the target base attack (refs *7* and *36* and Figure 11). Gln^{237} interacts with the orphan guanine and is thought to regulate the early steps in the base flipping process and the formation of intermediates **1** and **2** (*7*, *36*). Thus, alterations in interactions involving Gln^{237} may affect steps leading to intermediates **3A** and **3B** (Figure 2). Our observation that the pre-steady-state methylation rates with poly(dI-dC) are 2-fold slower than with poly(dG-dC) may therefore result from this missing hydrogen bond between Gln^{237} and the orphan inosine. In contrast, the enzyme−DNA interactions at Ile^{86} require that the active site loop is closed (ref *7* and Figure 11) with the cytosine positioned in the active site (i.e., intermediates **1** and **2** are formed (ref *7* and Figure 11)). Thus, a lack of interaction with Ile^{86} should not affect the steps leading to intermediates **3A** and **3B** but rather the stability of this active site loop in the closed position. The release of the active site loop is part of the product release process and the accompanying proton elimination steps (Figure 2, **3A** → **4A** and **3B** → **4B**). Thus, loop opening before methyl transfer may lead to uncontrolled solvent access to intermediate **2** (Figure 11 and ref *42*) and/or premature release of intermediates **1** and **2**. The excess tritium released during the methylation reaction with poly(dI-dC) (Figure 6A) is fully consistent with this scenario. The premature loop release prior to methyl transfer

can lead to uncontrolled protonation of intermediate **2**, and/or premature release of intermediates **1** and **2**, without the methyl transfer step. Similarly, loop release and uncontrolled solvent access to intermediate **2** are likely causes of the faster exchange rates with poly(dI-dC) in the presence of AdoHcy and *N*-methyl-AdoMet relative to poly(dG-dC (Table 1). In summary, comparison of poly(dG-dC) and poly(dI-dC) substrates is consistent with the stabilization of the active site loop through a hydrogen bond between Ile^{86} and guanine (ref *7* and Figure 11). Since intermediates **1** and **2** tend to accumulate prior to the slow methyl transfer step, the closure of the active site loop prevents premature release of the target base and uncontrolled solvent access at the reactive intermediate **2** (Figure 2). Blocking uncontrolled solvent access to intermediate **2** is important for minimizing both the exchange reaction and the mutagenic deamination (Figure 2, **1 → 2 → 3B → 4B)**.

The reactions with the poly(dI-dC) substrate also indicate that the loop closure can contribute to the slow steady-state step and to the early steps in target base recognition. The faster steady-state rates with no pre-steady-state burst in the reaction with poly(dI-dC) relative to poly(dG-dC) (Figure 4A vs Figure 6A and Figure 4B vs Figure 6B) are most likely caused by unstable active site loop, leading to faster product release (ref *7* and Figure 11). Moreover, the differences between poly(dG-dC) and poly(dI-dC) during processive catalysis (Figure 8A) suggest that the active site loop is partially closed with poly(dG-dC) after AdoHcy release, retaining the enzyme on the DNA. This is somewhat surprising since structural studies (ref *7* and Figure 11) suggest that the loop closure is primarily dependent on cofactor binding. In contrast, the relative instability of the loop and thus the M.HhaI·DNA complex with poly(dI-dC) results in the enzyme leaving prematurely and is thus less processive. Similarly, the large difference between poly(dG-dC) and poly(dI-dC) in the exchange rates in the absence of the cofactor is in a sharp contrast to the similar exchange rates in the presence of the cofactor (Table 1). We suggest that the low exchange rates with poly(dI-dC) in the absence of cofactor are due to the lack of both factors that control the closure of the active site loop: interaction at the Ile^{86} site and the cofactor binding (ref *7* and Figure 11).

Finally, these studies with poly(dG-dC) and poly(dI-dC) substrates offer some insights into the enzyme's role in the base flipping process (*8*, *15*, *34*). A passive mechanism involves the protein simply stabilizing the extrahelical target base which spontaneously becomes unstacked from the duplex DNA, while an active mechanism invokes participation of the enzyme in the unstacking process itself. The loss of one of the three hydrogen bonds per base pair in poly(dI-dC) should result in faster formation of intermediate **1** and **2**, if these intermediates are formed largely by a passive mechanism. Our observation of similar rates with poly(dI-dC) and poly(dG-dC) argues against a passive mechanism. Interestingly, we find the reverse is true with the mammalian enzyme (Dnmt1), which shows at least 10-fold higher catalytic rates with poly(dI-dC) than poly(dG-dC).[2]

Methylation and Exchange with the Gln^{237}Trp Mutant. Gln^{237} makes hydrogen bonds that are considered to be crucial for the base flipping process and stabilization of the extrahelical cytosine (Figure 11 and refs *7* and *36*). Earlier analysis (*19*) of 19 different Gln^{237} mutants showed that the methylation rates can be 2−33-fold slower than wild-type M.HhaI. The Gln^{237}Trp mutant is one of the least active (*19*), and based on the crystal structures (Figure 11 and refs *7* and *36*) these substitutions are thought to impact the enzyme's ability to form intermediate **1**. We were interested to see if the exchange reactions could be used to probe this prediction. We find that, similar to the exchange reaction in the absence of the cofactor (Figure 5B), the mutant clearly shows a pH-dependent change in SKIE. This is expected if the pH profiles and the measured pK_a are caused by the active site Cys^{81}, and if the reactions are limited by the cysteine nucleophilic attack and the conversion between intermediates **1** and **2**. None of the reactions with the mutant show a pH/SKIE response expected for a reaction that is *primarily* limited by the cysteine nucleophilic attack with the measured pK_a (dashed line, upper panel, in Figures 5, 7, and 9B). This is understandable since the conversion between intermediates **1** and **2** depends on a specific set of hydrogen bonds (Figure 2 and refs *7* and *18*) which may contribute to the SKIE (*46*). In summary, our results with the Gln^{237} mutant support our proposal that the pH/SKIE studies can be used to study the relationship between base flipping and catalysis. For a comparison, crystallographic (*34*) and fluorescence studies (*14*) reveal the extent of DNA deformation but do not monitor catalysis by Cys^{81}. ^{19}F NMR studies (*15*) do provide insights into intermediates **1** and **2** (Figure 2); however, the methyl transfer step at 5-fluorocytosine is exceptionally slow, which obscures the actual rates of conversion between intermediates. The pH/SKIE studies can be measured with any DNA substrate using routine methyltransferase assays.

In contrast to the wild-type enzyme, the exchange reaction with the mutant shows a notably decreased dependence on the cofactor analogues (Table 1). Thus, the mutation affects not only interactions with the orphan guanine but also interactions between intermediate **2** and the cofactor that take place in the active site. Since the enzyme's active site is 15 Å away from Gln^{237} (Figure 11), substitutions of Gln^{237} indirectly alter the network of hydrogen bonds (*36*) that position intermediates **1** and **2** in the active site. The results with the mutant also support our conclusions from poly(dI-dC) studies using the wild-type enzyme. The mutant shows no difference between the poly(dI-dC) and poly(dG-dC) substrates (Table 1 and Figure 9A), and both substrates show identical methylation and accompanying tritium release rates. As suggested above, the excess tritium release which occurs with the wild-type enzyme (Figure 6A) results from the destabilization of the active site loop and increased solvent access to reactive intermediate **2** (Figure 2) that accumulates prior to the slow methyl transfer step. Accumulation of intermediates **1** and **2** does not occur with the mutant since formation of intermediates **1** and **2** is the slow step (Figure 1).

Proton Inventory Studies. We used proton inventory analysis (Figure 10) in an attempt to further determine if different reactions share similar rate-limiting steps and catalytic intermediates. Proton inventory profiles are usually described according to their shape and calculated fractionation factors (eq 4 and ref *29*). The overall shape can indicate the number of steps controlling the rate-limiting step and SKIE and whether the SKIE is caused in the ground state, transition state, or both. The fractionation factors provide insights into functionalities causing the SKIE and can support

a comparison of different proton inventory profiles with numerical precision. While proton inventory results can be difficult to interpret precisely, we are primarily interested in their application to determine if the exchange reaction under different conditions follows similar mechanisms.

The proton inventory results support our earlier proposal that the methylation reactions with poly(dG-dC), poly(dI-dC), and Gln^{237}Trp depend on different rate-limiting steps. The pre-steady-state methylation rates with poly(dG-dC) depend on the methyl transfer step (Figure 2, **2** → **3A**), and no SKIE is observed (Figure 10A). The proton inventory for the methylation reaction with poly(dI-dC) (Figures 10B and 6A) results from the combined steps of methyl and proton transfer (Figure 2, **2** → **3A** and **2** → **3A**). The methylation reactions with the Gln^{237}Trp mutant and the wild-type enzyme without cofactor show similar proton inventory profiles, consistent with our earlier proposal that in both reactions the rate-limiting step is the nucleophilic attack by Cys^{81} (Figure 2, **1** → **2**).

The proton inventory profiles for the exchange reaction with sinefungin and poly(dI-dC) and poly(dG-dC) appear to be identical (Figure 10A,B and Table 2), indicating that the rate-limiting steps and catalytic mechanism are similar for these two reactions. The ϕ_T measured with sinefungin (Table 2) can be found in reactions where the rate-limiting step involves a proton bridge (N−H−C) in the transition state (ref *29*, pp 85 and 86). This is consistent with our proposal that the exchange reaction with sinefungin and both DNA substrates involves a direct interaction between the amino group on the cofactor and the C^5 on the target base. Moreover, similar proton inventory profiles are observed in the same reaction with Dnmt1,[2] indicating that M.HhaI and Dnmt1 follow very similar mechanisms with sinefungin.

The ϕ_T is similar in magnitude for the exchange reaction with *N*-methyl-AdoMet and sinefungin with poly(dG-dC) but not with poly(dI-dC) (Table 2). This is consistent with our proposal that the slow exchange reaction with *N*-methyl-AdoMet and poly(dG-dC) depends on the cofactor amino moiety, while the high exchange rates in the reaction with poly(dI-dC) and *N*-methyl-AdoMet (Table 1) result in part from the premature release of the active site loop, exposing intermediate **2** (Figure 2) to solvent molecules. The similar proton inventory profiles for the exchange reactions with AdoMet and *N*-methyl-AdoMet with poly(dI-dC) (Table 2) suggest that both reactions result from uncontrolled solvent access to intermediate **2**, caused by premature active site loop release. In summary, the proton inventory results support the proposed mechanism that tritium release by sinefungin and *N*-methyl-AdoMet is controlled by the cofactor and the active site loop.

The proton inventory profiles in the exchange reaction without cofactor and poly(dG-dC) and the exchange reactions with the Gln^{237}Trp mutant are dome shaped at pH 6.5 (data not shown) and partially curved (Figure 10C) at pH 8.0. Dome-shaped proton inventories which change with pH (Figures 5B and 9B) suggest that more than one step determines the rate-limiting step in those reactions (*29*), and that at least one is pH sensitive. This is consistent with our suggestion that nucleophlic attack by Cys^{81} is partially rate limiting in these reactions. If the pH-sensitive component of the SKIE is cysteine nucleophilic attack, the increase in SKIE caused by the increase in pH suggests that the nucleophilic cysteine is deprotonated in the transition state during the conversion between intermediates **1** → **2** (eq 4, ϕ_T, $n = 1$, $m = 0$). Thus, deprotonation of Cys^{81} occurs during the attack step, not prior. The pH-independent component of the SKIE shows an inverse SKIE which may involve one or more of the hydrogen bonds which activate intermediate **1** (*46*), since none of the functionalities on intermediates **1** and **2** are likely to cause such a fractionation factor when present alone (*29*). Finally, the reactions proposed to be limited by the **1** → **2** transition (Figure 10C), and reaction without cofactor and with poly(dG-dC), show an inverse SKIE and an apparent transition state fractionation factor (ϕ_T) of about 2 (Table 2). The reactions that are limited by proton transfer at intermediate **2** (**2** → **3B**) show a ground state fractionation factor ϕ_G around 2 (Figure 10A,B).

ACKNOWLEDGMENT

We gratefully acknowledge Ben Hopkins and Stephen Fiacco for their excellent help in these experiments and Drs. R. J. Roberts and S. Kumar from New England Biolabs for their generous gift of mutant M.HhaI plasmids.

REFERENCES

1. Jones, P. A., and Laird, P. W. (1999) Cancer epigenetics comes of age, *Nat. Genet. 21*, 163−167.
2. Jones, P. A., and Takai, D. (2001) The role of dna methylation in mammalian epigenetics, *Science 293*, 1068−1070.
3. Robertson, K. D., and Jones, P. A. (2000) DNA methylation: past, present and future directions, *Carcinogenesis 21*, 461−467.
4. Cheng, X., and Blumnethal, R. M. (1999) *S-Adenosylmethionine-Dependent Methyltransferases: Structures and Functions*, pp 1−400, World Scientific, Singapore, New Jersey, London, and Hong Kong.
5. Douglas, K. T. (1987) The thymidylate synthesis cycle and anticancer drugs, *Med. Res. Rev. 7*, 441−475.
6. Cheng, X., Kumar, S., Posfai, J., Pflugrath, J. W., and Roberts, R. J. (1993) Crystal structure of the HhaI DNA methyltransferase complexed with S-adenosyl-L-methionine, *Cell 74*, 299−307.
7. Klimasauskas, S., Kumar, S., Roberts, R. J., and Cheng, X. (1994) HhaI methyltransferase flips its target base out of the DNA helix, *Cell 76*, 357−369.
8. Cheng, X., and Roberts, R. J. (2001) AdoMet-dependent methylation, DNA methyltransferases and base flipping, *Nucleic Acids Res. 29*, 3784−3795.
9. Lindstrom, W. M., Jr., Flynn, J., and Reich, N. O. (2000) Reconciling structure and function in HhaI DNA cytosine-C-5 methyltransferase, *J. Biol. Chem. 275*, 4912−4919.
10. Vilkaitis, G., Merkiene, E., Serva, S., Weinhold, E., and Klimasauskas, S. (2001) The mechanism of DNA cytosine-5 methylation. kinetic and mutational dissection of Hhai methyltransferase, *J. Biol. Chem. 276*, 20924−20934.
11. Allan, B. W., Beechem, J. M., Lindstrom, W. M., and Reich, N. O. (1998) Direct real time observation of base flipping by the EcoRI DNA methyltransferase, *J. Biol. Chem. 273*, 2368−2373.
12. Allan, B. W., and Reich, N. O. (1996) Targeted base stacking disruption by the EcoRI DNA methyltransferase, *Biochemistry 35*, 14757−14762.
13. Allan, B. W., Garcia, R., Maegley, K., Mort, J., Wong, D., Lindstrom, W., Beechem, J. M., and Reich, N. O. (1999) DNA bending by EcoRI DNA methyltransferase accelerates base flipping but compromises specificity, *J. Biol. Chem. 274*, 19269−19275.
14. Holz, B., Klimasauskas, S., Serva, S., and Weinhold, E. (1998) 2-Aminopurine as a fluorescent probe for DNA base flipping by methyltransferases, *Nucleic Acids Res. 26*, 1076−1083.
15. Klimasauskas, S., Szyperski, T., Serva, S., and Wuthrich, K. (1998) Dynamic modes of the flipped-out cytosine during HhaI methyltransferase-DNA interactions in solution, *EMBO J. 17*, 317−324.
16. Finer-Moore, J. S., Santi, D. V., and Stroud, R. M. (2003) Lessons and conclusions from dissecting the mechanism of a bisubstrate

enzyme: thymidylate synthase mutagenesis, function, and structure, *Biochemistry 42*, 248−256.
17. Wu, J. C., and Santi, D. V. (1987) Kinetic and catalytic mechanism of HhaI methyltransferase, *J. Biol. Chem. 262*, 4778−4786.
18. Perakyla, M. (1998) A model study of the enzyme-catalyzed cytosine methylation using ab initio quantum mechanical and density functional theory calculations: pK_a of the cytosine N3 in the intermediates and transition states of the reaction, *J. Am. Chem. Soc. 120*, 12895−12902.
19. Mi, S., Alonso, D., and Roberts, R. J. (1995) Functional analysis of Gln-237 mutants of HhaI methyltransferase, *Nucleic Acids Res. 23*, 620−627.
20. Gabbara, S., Sheluho, D., and Bhagwat, A. S. (1995) Cytosine methyltransferase from *Escherichia coli* in which active site cysteine is replaced with serine is partially active, *Biochemistry 34*, 8914−8923.
21. Shen, J. C., Rideout, W. M. d., and Jones, P. A. (1992) High-frequency mutagenesis by a DNA methyltransferase, *Cell 71*, 1073−1080.
22. Zingg, J. M., Shen, J. C., and Jones, P. A. (1998) Enzyme-mediated cytosine deamination by the bacterial methyltransferase M.MspI, *Biochem. J. 332*, 223−230.
23. Zingg, J. M., Shen, J. C., Yang, A. S., Rapoport, H., and Jones, P. A. (1996) Methylation inhibitors can increase the rate of cytosine deamination by (cytosine-5)-DNA methyltransferase, *Nucleic Acids Res. 24*, 3267−3275.
24. Pfeifer, G. P., Tang, M., and Denissenko, M. F. (2000) in *DNA Methylation and Cancer* (Johns, P. A., and Vogt, P. K., Eds.) pp 1−19, Springer-Verlag, Berlin.
25. Reich, N. O., and Mashhoon, N. (1991) Kinetic mechanism of the EcoRI DNA methyltransferase, *Biochemistry 30*, 2933−2939.
26. Flynn, J., Glickman, J. F., and Reich, N. O. (1996) Murine DNA cytosine-C5 methyltransferase: pre-steady- and steady-state kinetic analysis with regulatory DNA sequences, *Biochemistry 35*, 7308−7315.
27. Johnson, K. A. (1992) in *The Enzymes* (Boyer, P. A., Ed.) Academic Press, New York.
28. Cornish-Bowden, A. (1999) *Fundamentals of Enzyme Kinetics*, Portland Press, Colchester, U.K.
29. Quinn, D. M., and Sutton, L. D. (1991) in *Enzyme Mechanism from Isotope Effects* (Cook, P. F., Ed.) pp 73−126, CRC Press, Boca Raton, FL.
30. Born, T. L., and Blanchard, J. S. (1999) Enzyme-catalyzed acylation of homoserine: mechanistic characterization of the *Escherichia coli* metA-encoded homoserine transsuccinylase, *Biochemistry 38*, 14416−14423.
31. Brocklehurst, K., Kowlessur, D., Patel, G., Templeton, W., Quigley, K., Thomas, E. W., Wharton, C. W., Willenbrock, F., and Szawelski, R. J. (1988) Consequences of molecular recognition in the S1-S2 intersubsite region of papain for catalytic-site chemistry. Change in pH-dependence characteristics and generation of an inverse solvent kinetic isotope effect by introduction of a P1−P2 amide bond into a two-protonic-state reactivity probe, *Biochem. J. 250*, 761−772.
32. Kinch, L. N., and Phillips, M. A. (2000) Single-turnover kinetic analysis of *Trypanosoma cruzi* S-adenosylmethionine decarboxylase, *Biochemistry 39*, 3336−3343.
33. Scheuring, J., and Schramm, V. L. (1997) Pertussis toxin: transition state analysis for ADP-ribosylation of G-protein peptide alphai3C20, *Biochemistry 36*, 8215−8223.
34. O'Gara, M., Horton, J. R., Roberts, R. J., and Cheng, X. (1998) Structures of HhaI methyltransferase complexed with substrates containing mismatches at the target base, *Nat. Struct. Biol. 5*, 872−877.
35. Renbaum, P., and Razin, A. (1992) Mode of action of the Spiroplasma CpG methylase M.SssI, *FEBS Lett. 313*, 243−247.
36. Huang, N., Banavali, N. K., and MacKerell, A. D., Jr. (2003) Protein-facilitated base flipping in DNA by cytosine-5-methyltransferase, *Proc. Natl. Acad. Sci. U.S.A. 100*, 68−73.
37. Ivanetich, K. M., and Santi, D. V. (1992) 5,6-dihydropyrimidine adducts in the reactions and interactions of pyrimidines with proteins, *Prog. Nucleic Acid Res. Mol. Biol. 42*, 127−156.
38. Yoder, J. A., Soman, N. S., Verdine, G. L., and Bestor, T. H. (1997) DNA (cytosine-5)-methyltransferases in mouse cells and tissues. Studies with a mechanism-based probe, *J. Mol. Biol. 270*, 385−395.
39. Szyf, M. (1996) The DNA methylation machinery as a target for anticancer therapy, *Pharmacol. Ther. 70*, 1−37.
40. O'Gara, M., Klimasauskas, S., Roberts, R. J., and Cheng, X. (1996) Enzymatic C5-cytosine methylation of DNA: mechanistic implications of new crystal structures for HhaL methyltransferase-DNA-AdoHcy complexes, *J. Mol. Biol. 261*, 634−645.
41. O'Gara, M., Zhang, X., Roberts, R. J., and Cheng, X. (1999) Structure of a binary complex of HhaI methyltransferase with S-adenosyl-L-methionine formed in the presence of a short nonspecific DNA oligonucleotide, *J. Mol. Biol. 287*, 201−209.
42. Lau, E. Y., and Bruice, T. C. (1999) Active site dynamics of the HhaI methyltransferase: insights from computer simulation, *J. Mol. Biol. 293*, 9−18.
43. Schowen, R. L. (1977) Isotope effects on enzyme-catalyzed reactions, in *Proceedings of the Sixth Annual Harry Steenbock Symposium* (Cleland, W. W., Northrop, D. B., and O'Leary, M. H., Eds.) Madison, WI, June 4 and 5, 1976, pp 64−99, University Park Press, Baltimore, MD.
44. Vilkaitis, G., Dong, A., Weinhold, E., Cheng, X., and Klimasauskas, S. (2000) Functional roles of the conserved threonine 250 in the target recognition domain of HhaI DNA methyltransferase, *J. Biol. Chem. 275*, 38722−38730.
45. Kumar, V. D., Harrison, R. W., Andrews, L. C., and Weber, I. T. (1992) Crystal structure at 1.5-Å resolution of d(CGCICICG), an octanucleotide containing inosine, and its comparison with d(CGCG) and d(CGCGCG) structures, *Biochemistry 31*, 1541−1550.
46. Cleland, W. W. (1992) Low-barrier hydrogen bonds and low fractionation factor bases in enzymatic reactions, *Biochemistry 31*, 317−319.

BI0496743